Numerical investigation of enhanced femtosecond supercontinuum via a weak seed in noble gases

C. Shanor,[1] T. Ensley,[2] D. J. Hagan,[2] E. W. Van Stryland,[2] E. M. Wright,[1] and M. Kolesik[1,*]

[1] *College of Optical Sciences, University of Arizona, 1630 East University Boulevard, Tucson, Arizona 85721 USA*

[2] *College of Optics & Photonics: CREOL & FPCE, University of Central Florida, 4000 Central Florida Blvd., Orlando, Florida 32816-2700, USA*

[*] *kolesik@optics.arizona.edu*

Abstract: Numerical simulations are employed to elucidate the physics underlying the enhanced femtosecond supercontinuum generation previously observed during optical filamentation in noble gases and in the presence of a weak seed pulse. Simulations based on the metastable electronic state approach are shown not only to capture the qualitative features of the experiment, but also reveal the relation of the observed enhancement to recent developments in the area of sub-cycle engineering of filaments.

OCIS codes: (320.6629) Supercontinuum generation; (190.5940) Self-action effects.

References and links

1. For a comprehensive overview see, D. Faccio, A. Couairion, and P. Di Trapani, *Conical Waves, Filaments and Nonlinear Filamentation Optics* (Aracne Editrice Rome, 2007).
2. M. Kolesik, E. M. Wright, and J. V. Moloney, "Interpretation of the spectrally resolved far field of femtosecond pulses propagating in bulk nonlinear dispersive media," Opt. Express **13**, 10729–10741 (2005).
3. M. Kolesik, and J. V. Moloney, "Perturbative and non-perturbative aspects of optical filamentation in bulk dielectric media," Opt. Express **16**, 2971–2988 (2008).
4. P. Béjot, G. Karras, F. Billard, E. Hertz, B. Lavorel, E. Cormier, and O. Faucher, "Harmonic generation and nonlinear propagation: When secondary radiations have primary consequences," Phys. Rev. Lett. **112**, 203902 (2014).
5. P. Béjot, G. Karras, F. Billard, J. Doussot, E. Hertz, B. Lavorel, and O. Faucher, "Sub-cycle engineering of laser filamentation in gas by harmonic seeding," Phys. Rev. A **92**, 053417 (2015).
6. J. Doussot, P. Béjot, G. Karras, F. Billard, and O. Faucher, "Phase control of two-color filamentation," J. Phys. B: Atom. Mol. Opt. Phys. **48**, 184005 (2015).
7. J. Doussot, P. Béjot, and O. Faucher, "Impact of third-harmonic generation on the filamentation process," Phys. Rev. A **93**, 033857 (2016).
8. E. E. Serebryannikov and A. M. Zheltikov, "Strong-field photoionization as excited state tunneling," Phys. Rev. Lett. **116**, 123901 (2016).
9. M. Kolesik, J. M. Brown, A. Teleki, P. Jakobsen, J. V. Moloney, and E. M. Wright, "Metastable electronic states and nonlinear response for high-intensity optical pulses," Optica **1**, 323–331 (2014).
10. J. M. Brown, C. Shanor, E. M. Wright, and M. Kolesik, "Carrier-wave shape effects in optical filamentation," Opt. Lett. **41**, 859 (2016).
11. T. R. Ensley, D. A. Fishman, S. Webster, L. A. Padilha, D. J. Hagan, and E. W. Van Stryland, "Energy and spectral enhancement of femtosecond supercontinuum in a noble gas using a weak seed," Opt. Express **19**(2), 757–763 (2011).
12. T. R. Ensley, "White light continuum for broadband nonlinear spectroscopy," Ph.D. thesis, CREOL, The College of Optics and Photonics (2015).

#264346 Received 29 Apr 2016; revised 16 Jun 2016; accepted 17 Jun 2016; published 24 Jun 2016

13. F. Théberge, N. Aközbek, W. Liu, A. Becker, and S.L. Chin, "Tunable ultrashort laser pulses generated through filamentation in gases," Phys. Rev. Lett. **97**, 023904 (2006).
14. X. M. Tong and C. D. Lin, "Empirical formula for static field ionization rates of atoms and molecules by lasers in the barrier-suppression regime," J. Phys. B. **38**, 2593 (2005).
15. H. J. Lehmeir, W. Leupacher, and A. Penzkofer, "Nonresonant third order hyperpolarizability of rare gases and N_2 determined by third harmonic generation," Opt. Commun. **56**, 67 (1985).
16. M. Kolesik and J. V. Moloney, "Nonlinear optical pulse propagation simulation: From Maxwell's to unidirectional equations", Phys. Rev. E. **70** 036604 (2004).
17. J. Andreasen, and M. Kolesik, "Nonlinear propagation of light in structured media: Generalized unidirectional pulse propagation equations", Phys. Rev. E **86**, 036706 (2012).
18. http://acms.arizona.edu/FemtoTheory/MK_personal/guppelab/

1. Introduction

The theory and accompanying experiments regarding the phenomenon of weak radiation generation during the optical filamentation of ultrashort pulses in atomic gases are now well documented [1]. In the effective three-wave mixing picture [2] of this phenomenon the optical filament is viewed as an optical wave-packet localized in space and time, formed by the complex interplay between diffraction, group-velocity dispersion, nonlinear self-focusing, and plasma generation and defocusing. This resulting near solitary wave describing the filament in turn produces a moving refractive-index perturbation from which weak waves can scatter, giving rise to the growth of weak radiation according to phase-matching conditions dependent on the detailed dispersion landscape for the medium. The weak radiation generated in this manner is responsible for the detailed features of a range of phenomena in atomic gases and condensed media alike, including supercontinuum (SC) or white light continuum (WLC) generation, and conical waves such as X-waves and O-waves [3].

A series of recent theoretical and experimental works have shown that the interaction between an optical filament and an externally applied weak seed, a variant of the situation discussed above, can give rise to sub-cycle engineering of the filament [4–7]. In particular, it was shown that adding a weak third-harmonic seed pulse can be used to alter the propagation characteristics, SC generation, and plasma generation for optical filaments that are orders of magnitude stronger. Using numerical solutions of the time-dependent Schrödinger equation, Bejot *et. al* [5] traced this enhancement to interference between ionization channels involving different color photons, highlighting that this is a quantum coherent effect rooted in the extreme nature of the off-resonant light-matter interaction, see also the recent Ref. [8]. In subsequent work some of the present authors (CS,EMW,MK) showed that the enhancement could also be explained in the framework of the Metastable Electronic State Approach (MESA) [9], in which the atomic state is represented in terms of the metastable, or resonance, states for the atom in the off-resonant field [10]. The MESA view highlights the relation of the enhancement to the carrier-wave shape, and the occurrence of local temporal peaks, which depends critically on the relative phase between the carrier waves of the filament and weak seed pulse.

In the present paper we examine an earlier set of experiments by some of the present authors (TRE,DJH,EVS) that reported enhanced SC generation in noble gases, but for seed wavelengths closer to the filament, see Refs. [11,12] for details. More specifically, Fig. 1 shows experimental SC spectra for the case of Krypton gas, a filament of center wavelength 780 nm, and seed wavelengths of 600 nm (left plot) and 1300 nm (right plot). The filament or pump energy was 0.4 mJ and the seed energy 1 μJ, and the pump and seed pulses were overlapped spatially and temporally in the noble gas chamber. The experimental SC spectra extended up to 1400 nm and was limited to greater than 300 nm by the notch filter employed. Furthermore there are gaps in the experimental data appearing in the vicinity of the pump ($750-810$ nm) and the seed ($550-650$ nm for the 600 nm seed and $1240-1340$ nm for the 1300 nm seed), these being indicated by the gray areas. Each plot shows the angle integrated SC energy density in nJ/nm versus

#264346 Received 29 Apr 2016; revised 16 Jun 2016; accepted 17 Jun 2016; published 24 Jun 2016

wavelength both with (red data points) and without (black data points) the seed present. Key features that have remained without detailed explanation are why the enhancement occurs at all in this experiment, the spectral distribution of the SC, and why it occurs for the 600 nm seed but not for the 1300 nm seed. The authors of Ref. [11] stressed the critical role played by four-wave-mixing (FWM) and we shall elucidate on this here. Earlier simulations of the above experiment by B. Shim, S. E. Schrauth, and Alex Gaeta of Cornell University, also alluded to the role of FWM in the SC generation process. These simulations are reported in the thesis of Ref. [12] but have not been published in an archival journal. A somewhat similar role was played by FWM in the experiment reported in [13], which demonstrated efficient, filament-aided conversion of mid-infrared radiation into the visible. The features that distinguish the physics discussed here are that the seed energies are exceedingly small, and that the supercontinuum enhancement extends well beyond the discrete frequencies dictated by the FWM process.

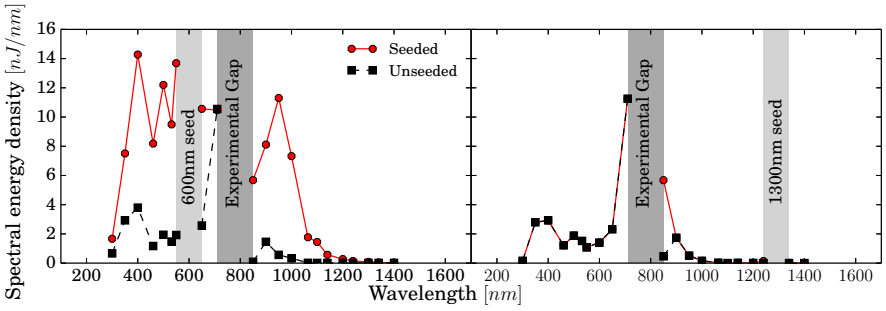

Fig. 1. Angle integrated SC energy density in nJ/nm versus wavelength both with (red data points) and without (black data points) the seed applied. The left plot is for a seed wavelength of 600 nm and the right plot for 1300 nm. The gray regions indicate gaps in the experimental data in the vicinity of the pump and seed pulses. The data is adapted from that given in Fig. 2 of Ref. [11].

This experiment predates the enhancement experiments described in the second paragraph above, and attracts particular attention due to the potential as an alternative to conventional sources of radiation for applications such a nonlinear spectroscopy. Here using numerical simulations based on MESA we demonstrate that we can capture the qualitative features of the SC spectra for this experiment, in particular the relevance of the seed wavelength to the enhancement. Furthermore, we find that the enhancement is sensitive to the carrier-wave shape offering the possibility that the white-light spectral power can be optimized in a given wavelength interval. This observation may be important for future applications. Finally we allude to the applicability of our findings to other noble gases.

2. Supercontinuum spectra for Krypton gas

We employ numerical simulations of optical filamentation with a two-color pulse comprising both pump and seed with full spatial and temporal resolution. More specifically, for the atomic model we employ a quasi-static approximation based on the single-state MESA (ssMESA) [9], and employing Single Active Electron (SAE) models of noble gas atoms utilizing the SAE potentials given in [14]. This procedure yields the nonlinear polarization, related to the change in refractive-index, and the ionization rate, both as functions of the electric field strength. This approach is microscopically self-consistent in the sense that the derived nonlinear polarizations and ionization rates are automatically in correct proportion. To complete the specification of the optical properties the linear data are incorporated using the known dispersion relation for noble

#264346 Received 29 Apr 2016; revised 16 Jun 2016; accepted 17 Jun 2016; published 24 Jun 2016

gases [15]. The carrier resolved field propagation is then performed using the gUPPEcore [16, 17] pulse propagation solver [18] coupled to the ssMESA data.

Before discussing the results, we remark that we also performed extensive simulations with the classical model for optical filamentation, in which the nonlinear polarization is proportional to $E^3(t)$, and the nonlinear response due to ionization is parameterized by a power-law rate, with the free electrons giving rise to a Drude current. This classical filamentation model is also capable of reproducing some of the experimental results discussed here. Indeed the simulations by B. Shim, S. E. Schrauth, and A. Gaeta reported in the thesis of Ref. [12], but not published, allude to such agreement. However, we found that the classical approach requires parameter fine-tuning (the nonlinear Kerr coefficient, the order and coefficient for multi-photon ionization etc.) and even for optimal parameter sets some of the features and connections to the experiment are less robust. In particular, we found that the dependence of the SC enhancement on the seed energy is significantly underestimated in the classical model. The classical model therefore requires quite higher seed energies to mirror the experimental data at small seed intensities, while in the experiment the signal first grows faster with increasing seed energy and only later saturates (see Section 3).

In contrast, the ssMESA is free from the parameter uncertainties associated with the classical model. While it is fair to say that it is still not a *quantitative* theory, the fact that all qualitative features of the SC enhancement experiment can be reproduced with no parameters to adjust indicates that it as a suitable tool to explore the underlying physics of the SC enhancement. Because our focus here is not a comparative study of the two models, only the results obtained from the ssMESA based simulations will be discussed in what follows.

We focus attention in this Section on the case of SC generation in Krypton gas as that was the gas used in the experiment reported in Ref. [11]. In particular we have incorporated the parameters from that experiment, as documented in Ref. [12], into our simulations. Specifically, the pump pulse entering the gas chamber was chosen as Gaussian with spot size $w_p = 1300\ \mu$m, duration $t_p = 150$ fs, energy 0.4 mJ, and center wavelength 780 nm. The seed pulse was selected to overlap the pump pulse spatially and temporally half-way along the simulated chamber length of 40 cm held at a pressure of 3.7 atm, the seed energy being 1 μJ. This yields an optical filament of approximately $L_{fil} \sim 5$ cm length starting around $z = 28$ cm as inferred from the simulations (see Sec. 4 for a discussion), and the SC generation is assessed at the end of the chamber. Figure 2 shows the profiles of the angle-integrated SC spectra versus wavelength for the 600 nm seed (left plot) and the seed centered at 1300 nm (right plot). (As is usual we focus on the profile of the SC spectrum as opposed to the absolute yield as the latter is very sensitive to the detailed parameters.) For each case the black line indicates the SC spectrum without the seed present. As opposed to the experimental results shown in Fig. 1 the SC spectrum is shown on a log scale: This allows us to visualize the pump, seed, and SC on the same spectral plot, and also to look beyond the wavelength limit of the experiment, where the notch filtered limited observations to wavelengths greater than 300 nm. The experimental gaps around the pump ($710-850$ nm) and seed ($550-650$ nm for the 600 nm seed and $1240-1340$ nm for the 1300 nm seed) are indicated by gray regions in each plot.

The results in Fig. 2 show reasonable qualitative agreement with the experimental results displayed in Fig. 1. First, it is clear that once one accounts for the experimental pump and seed gaps there is little enhancement of the SC generation due to the presence of the seed for the 1300 nm wavelength in comparison to the 600 nm seed. Second, for the 600 nm case there are oscillations in the enhanced spectrum in the presence of the seed for wavelengths shorter than the gap around the seed, and a peak appearing for wavelengths larger than the pump gap. The simulations therefore capture two key qualitative features of the Krypton experiment [11].

#264346 Received 29 Apr 2016; revised 16 Jun 2016; accepted 17 Jun 2016; published 24 Jun 2016

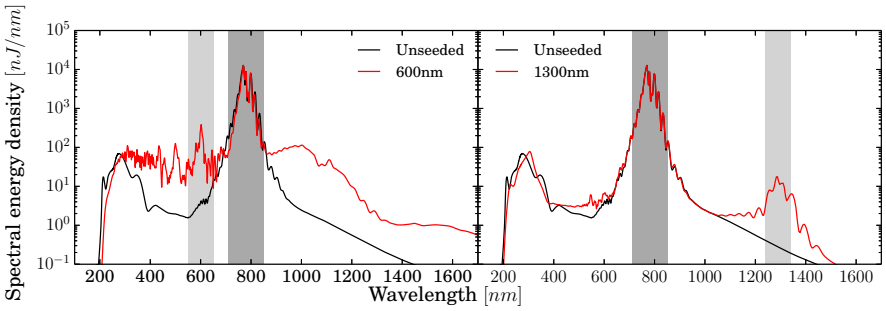

Fig. 2. Simulated angle-integrated SC spectra versus wavelength for the 600 nm seed (left plot) and the seed centered at 1300 nm (right plot). The gray regions indicate the experimental gaps around the pump (710 – 850 nm) and seed pulses (550 – 650 nm for the 600 nm seed and 1240 – 1340 nm for the 1300 nm seed).

3. Spectral enhancement

We next look at the spectral enhancement in more detail for the Krypton simulations in comparison to the experiment. The coarsest measure of the enhancement is to look at the ratio of the wavelength integrated SC generation both with and without the seed present, removing the experimental gaps to conform to the experimental situation. This was measured in the experiment as a function of the seed wavelength and is tabulated in the last column of Table 1 of Ref. [11] for a seed energy of 1 μJ. This enhancement is plotted versus seed wavelength in Fig. 3(a) as the red line, with a peak enhancement of around 3 for a seed wavelength of around 650 nm. The blue line in Fig. 3(a) is the corresponding result from the simulations obtained using the previous parameters, and this shows a peak enhancement of around 5.4 for a seed wavelength of around 650 nm. The simulations are therefore in reasonable qualitative agreement with the experiment: The larger enhancement from the simulations is not surprising given that deviations from exact beam alignment etc. could easily reduce the observed enhancement. We note that both the experiment and simulations show negligible enhancement for the 1300 nm seed.

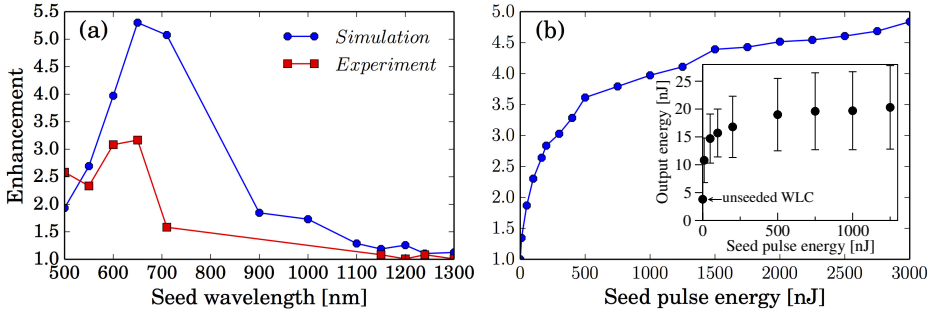

Fig. 3. Enhancement of the SC generation. a) The red line shows the experimental results from Ref. [11] for the enhancement as a function of seed wavelength with a peak enhancement of around 3 for a seed wavelength of around 650 nm. The blue line shows the corresponding result from the simulations, and shows a peak enhancement of around 5.4 for a seed wavelength of around 650 nm. b) Enhancement versus seed energy for a wavelength of 600 nm. For both cases the seed energy is 1 μ J. The inset shows the experimental data from Ref. [11] (see text for details).

#264346 Received 29 Apr 2016; revised 16 Jun 2016; accepted 17 Jun 2016; published 24 Jun 2016

As a further study Fig. 3(b) shows the enhancement obtained in the same manner as above but versus seed energy for a wavelength of 600 nm. This figure is reminiscent of the experimental Fig. 5 of Ref. [11], for which the corresponding data set is reproduced in the inset. It, too, shows output energy versus seed energy, but with an important difference: In Fig. 5 the energy collected is in the narrow spectral region 532 ± 4 nm [11], whereas for Fig. 3(b) the energy is assessed over all the full wavelength range minus the experimental gaps. Indeed we could not reproduce Fig. 5 of Ref. [11] with our simulations, but rather saw oscillations in output energy with seed pulse energy over the 8 nm window of the experiment.

The reason for our inability to reproduce Fig. 5 of Ref. [11] is actually an important finding from our simulations. So far we have tacitly assumed a fixed relative phase ϕ between the carrier waves of the pump and seed waves, $\cos(k_{Pump}z - \omega_{Pump}t)$ and $\cos(k_{Seed}z - \omega_{Seed}t + \phi)$, respectively: Note that this does not imply a fixed phase relationship between the pump and seed, and the instantaneous phase between the pump and seed waves changes with time and also evolves during the propagation. Figure 4(a) shows the angle integrated spectra versus wavelength obtained for $\phi = 0, \pi/5, \pi/2$, as well as the unseeded case, and plot (b) shows the corresponding integrated energy in the small range 535 ± 5 nm, normalized to the value for $\phi = 0$, versus the relative phase. Here we clearly see that the energy so calculated depends on the relative phase. (In contrast the results in Fig. 3 are relatively insensitive to the relative phases as they are integrated over a large spectral window.) Now, in the experiment the pump and seed waves are spatially and temporally overlapped in terms of their envelopes, but no effort was made to control this at the level of the relative phase of the carrier waves. Furthermore, the experimental spectra are averaged over many shots, so it is reasonable that the results in Fig. 5 of Ref. [11] are an ensemble average over the relative phase of the carrier waves. We remark that we obtain results similar to Figure 4(a) if the relative phase remains fixed but the pump energy is varied by a small amount. The key point is that the experimental results are an ensemble average over realizations, whereas our simulations are single shot. We have refrained from performing the ensemble average numerically due to the lack of detailed knowledge of the pump and seed pulse fluctuations and also the prohibitive computational time required (tens to hundreds of realizations would be needed each taking many hours).

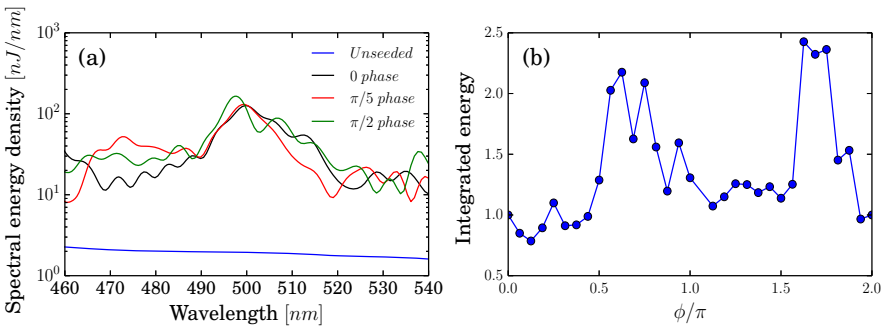

Fig. 4. a) Angle integrated spectra obtained for relative phases ϕ of 0 (black), $\pi/5$ (red), $\pi/2$ (green), as well as the unseeded case (blue), and b) integrated energy in the wavelength range 535 ± 5 nm, normalized to the value for $\phi = 0$, versus the relative phase ϕ.

The sensitivity of the SC spectra to the relative phase between the carrier waves of the pump and seed is a signature that the carrier-wave shape is playing a role in the propagation characteristics and plasma generation of the optical filament, leading to enhanced SC generation. Depending on the relative phase between the constituent waves with different wavelengths, the local electric field maximum of the composite carrier wave can become more

#264346 Received 29 Apr 2016; revised 16 Jun 2016; accepted 17 Jun 2016; published 24 Jun 2016

peaked or flat. The resulting change in the local field modifies both the electronic Kerr response, and the local ionization rate. Both effects can accumulate and influence the pulse propagation despite the fact that the local field changes are relatively small. This is analogous to the recently studied case where the weak seed was at the third-harmonic, enabling systematic diagnostics to be performed on the plasma generation and SC enhancement [5]. In that work it was argued that the phase sensitivity will survive under propagation if the filament length $L_{fil} \ll \ell_{reph}$ is much shorter than the rephasing length between the pump and seed given by

$$\ell_{reph} = \lambda_{Seed} \left| \frac{1}{n_{Seed} - n_{Pump}} \right|, \tag{1}$$

so that the pump and seed remain in relative phase over the filament length. On the contrary if $L_{fil} \gg \ell_{reph}$ the phase sensitivity will be washed out under propagation. For the experiment under consideration we find $L_{fill} \sim 5$ cm (see Sec. 4), and using the dispersion data for Krypton [15] gives $\ell_{reph} \sim 5.2$ cm for the 600 nm seed, and $\ell_{reph} \sim 12.6$ cm for the 1300 nm seed. Thus the current experiment is in the intermediate regime with $L_{fil} \sim \ell_{reph}$ so that some level of sensitivity to the relative phase can survive as demonstrated by the simulations.

In the present case it is clear from Fig. 4(b) that the relative phase ϕ between the carrier waves could be used as a control knob to optimize SC generation within a spectral window a few nanometers wide. Thus control of the relative phase and subsequent SC modification presents an opportunity to increase the enhancement seen in the experiment of Ref. [11] if sufficient control could be exacted over the pump and seed pulses. Importantly, the relative pump-seed phase can be utilized to tune-up the generated white-light power by up to 100%-200% in a given target wavelength interval. This may increase the potential of this system as an alternative to conventional sources of radiation for applications such a nonlinear spectroscopy.

4. Role of four-wave mixing

Next we address the issue of why enhanced SC generation appears for the 600 nm seed and not the 1300 nm seed, as reflected in Figs. 1-3. In particular Fig. 3(a) shows that both experimentally and theoretically the enhancement maximizes at around a seed wavelength of 650 nm and falls off with increasing seed wavelength. What is a priori clear is that in our simulations the distinction between the two seed wavelengths cannot be rooted in some extreme light-matter interaction: The ssMESA model employed gives the nonlinearity as a function of the instantaneous electric field, so that within the quasi-static approximation the light-matter interaction is nearly blind to the photon colors involved. Post-adiabatic correction can improve the MESA-based model to account for delayed interactions and wavelength-dependent ionization, but they are not included here in the single-state treatment; This is why we can conclude that the physics is mainly driven by the local electric field intensity changes due to seeding, and not by some complex interplay between different-color fields.

Here we demonstrate numerically that the distinction between the two seed wavelengths lies in the process of four-wave-mixing (FWM) and associated phase-matching. If we denote the pump and signal wavelengths by $\lambda_{Pump} = 780$ nm and λ_{Seed}, then FWM involving two pump photons and one seed photon can yield a FWM signal with wavelength λ_{FWM} determined by $\lambda_{FWM}^{-1} = 2\lambda_{Pump}^{-1} - \lambda_{Seed}^{-1}$. For a collinear interaction of the waves the phase-matching condition is $\Delta k = 2k_{Pump} - k_{Seed} - k_{FWM} = 0$, where $k_\mu = 2\pi n_\mu/\lambda_\mu$, μ =Pump, Seed, FWM, n_μ being the refractive-index for the wavelength λ_μ. Using the known dispersion relation for Krypton it is found that collinear phase-matching of the FWM is not possible [15]. However, non-collinear phase-matching can occur, and using the law of cosines the required angle θ between the pump

#264346 Received 29 Apr 2016; revised 16 Jun 2016; accepted 17 Jun 2016; published 24 Jun 2016

and seed wavevectors is given by

$$\cos(\theta) = \frac{4k_{Pump}^2 + k_{Seed}^2 - k_{FWM}^2}{4k_{Pump}k_{Seed}}. \quad (2)$$

For the case of Krypton with $\lambda_{Seed} = 600$ nm we find $\lambda_{FWM} = 1114$ nm and $\theta_{600} = 0.0022$ rad, whereas for $\lambda_{Seed} = 1300$ nm we find $\lambda_{FWM} = 557$ nm and $\theta_{1300} = 0.0062$ rad, a three-fold increase in the required angle between the pump and seed wavevectors for phase-matching. The geometry for the two different seed wavelengths is illustrated in Fig. 5, for (a) 600 nm, and (b) 1300 nm, and highlights the larger angle required for the 1300 nm seed wavelength. Note that since this non-collinear FWM is phase-matched the corresponding coherence length is infinite, and this underpins why the rephasing length in Eq. (1) is the relevant spatial scale.

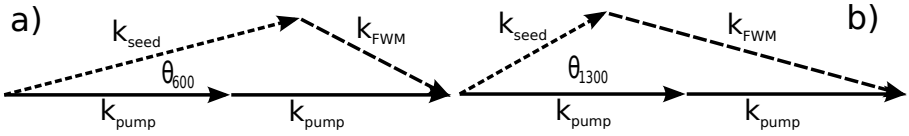

Fig. 5. Non-collinear phase-matching of the FWM for seed wavelengths of (a) 600 nm, and (b) 1300 nm. For purposes of illustration the angles θ_{600} and θ_{1300} between the pump and probe are exaggerated.

The above analysis is for plane-waves whereas the experiment involves a filament of width $w \sim 50$ μm (diameter 100 μm) as determined from the simulations. The angular spread of the optical filament is therefore of the order of $\theta_{fil} \sim \frac{\lambda_{Pump}}{\pi w} \sim 0.005$. To assess the relevance of FWM this angular spread is compared with θ from above: Then for the 600 nm seed the angular spread of the propagating fields can easily accommodate that needed for the FWM process $\theta_{600} = 0.002 < \theta_{fil}$, and we expect non-collinear phase-matched FWM to occur: This will lead to both on-axis and off-axis FWM as the pump and seed beams have a spread of angles. In contrast, for the 1300 nm seed $\theta_{1300} = 0.006 \sim \theta_{fil}$, so we expect FWM to play a relatively minor role.

We contend that the above phase-matching picture explains the presence (600 nm seed) or absence (1300 nm seed) of enhanced SC generation compared to the unseeded case. First, for the 1300 nm seed we argue that FWM does not play a role so we expect that the SC generation to be the same as the unseeded case. Second, for the 600 nm seed case the FWM can grow during propagation prior to filamentation and prolific SC generation, producing new frequencies via cascading over and above the pump and seed, and this acts as a catalyst that boosts the SC generation once it starts. To demonstrate this numerically Fig. 6 contains Visualization 1 of the angularly resolved logarithmic power spectrum $\log|E(k_\perp, \omega, z)|^2$ as the propagation distance z is varied, obtained by Fourier transforming the propagating field along the chamber length into the transverse wavenumber $k_\perp$ and angular frequency ω, for the unseeded case (left), 600 nm seed (center), and the 1300 nm seed (right). The angularly resolved power spectrum is a very useful diagnostic tool that not only displays the frequency content of the propagating field but also the associated transverse wavevectors $k_\perp$ that correlate with on-axis ($k_\perp = 0$) and off-axis emission directions in the far field. The stills shown in Fig. 6 are the angularly resolved spectra at the exit of the chamber: In all cases the pump has frequency $\omega_{Pump} = 2.4 \times 10^{15}$ rad/s, whereas the seed frequency is $\omega_{Seed} = 3.14 \times 10^{15}$ rad/s for seed wavelength 600 nm and $\omega_{Seed} = 1.45 \times 10^{15}$ rad/s for 1300 nm. First we note the clear similarity between the unseeded case (left) and the 1300 nm seed case (right), and viewing the animation shows that the SC generation proceeds in much the same way in both cases: Concentrating on the

#264346 Received 29 Apr 2016; revised 16 Jun 2016; accepted 17 Jun 2016; published 24 Jun 2016

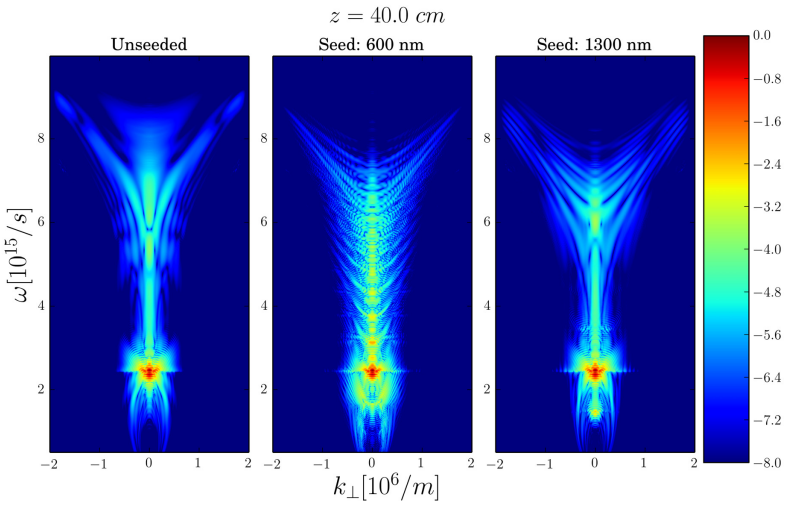

Fig. 6. Visualization 1. Animation of the evolution of the angularly resolved power spectrum $|E(k_\perp,\omega,z)|^2$ (on log scale), obtained by Fourier transforming the propagating field along the chamber length into the transverse wavenumber $k_\perp$ and angular frequency ω, for the unseeded case (left), 600 nm seed (center), and the 1300 nm seed (right). The stills are for the case at the exit of the noble gas chamber.

unseeded animation, the angularly resolved spectrum consists of waves centered around the pump ($\omega_{Pump} = 2.4 \times 10^{15}$ rad/s) and third harmonic (7.2×10^{15} rad/s) up to a propagation distance of around 28 cm. Past this point the spectrum starts to become rapidly populated between the pump and third harmonic, a process of prolific SC generation that persists until around 33 cm. Since SC generation is intimately tied to optical filamentation for propagation in bulk gases, we identify the start of the filament at around 28 cm, and the terminus at around 33 cm, yielding an estimate of the filament length as $L_{fil} \sim 5$ cm. We note that this estimate of the filament length would vary some depending on the criterion, for example, the length of the induced plasma channel, but this qualitative picture will suffice for our purposes.

In contrast, for the 600 nm seed case, even for the still, there is clear evidence of several on-axis peaks along $k_\perp = 0$, and these arise from FWM. The structure revealed in the angularly resolved spectrum is called a 'fish-wave' as it displays a fish bone-like structure due to the on-axis and off-axis FWM that is noticeably absent from the unseeded case [1]. This is clearly seen by viewing the animation for this case (center): At the start the pump ($\omega_{Pump} = 2.4 \times 10^{15}$ rad/s) and seed ($\omega_{Seed} = 1.45 \times 10^{15}$ rad/s) are present, but as the propagation proceeds the first FWM peak ($\omega_{FWM} = 1.7 \times 10^{15}$ rad/s) appears, along with some third-harmonic (7.2×10^{15} rad/s), followed by cascaded FWM, and then the SC generation kicks in around 28 cm and is clearly influenced, indeed enhanced. These simulations elucidate the role played by FWM in the enhanced SC generation, as conjectured in Ref. [11].

5. Other noble gases

To finish we demonstrate that the enhanced SC generation captured by our simulations for Krypton also appears for other noble gases. Experiments were carried out for Argon and Xenon, but the parameters needed for detailed simulations were not as extensively documented in this case [12], so we satisfy ourselves by showing some generic SC spectra for these gases. Figure 7 shows the simulated SC spectra for both Argon (left plot) and Xenon (right plot) for seeds

#264346 Received 29 Apr 2016; revised 16 Jun 2016; accepted 17 Jun 2016; published 24 Jun 2016

with wavelengths of 650 nm and 680 nm, respectively. In each case the unseeded case is shown for comparison, and we see features very similar to Fig. 2 for Krypton.

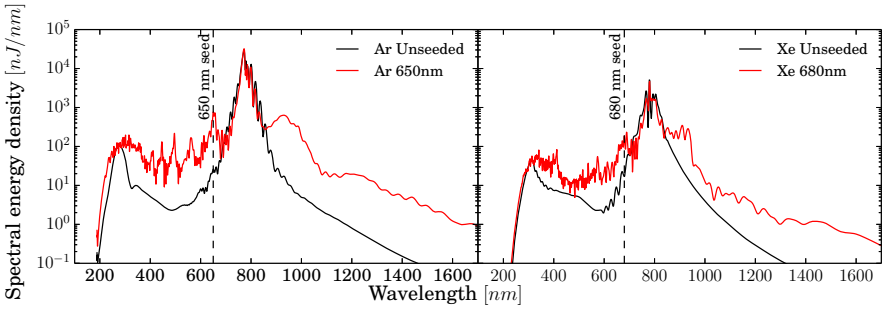

Fig. 7. Simulated spectra show a roughly order of magnitude enhancement of the supercontinuum radiation for Argon (left plot) and Xenon (right plot) for seeds with wavelengths of 650 nm and 680 nm, respectively.

We emphasize that while our simulation results can not be considered for *quantitative* comparisons against the experiment, the fact that the model does not rely on any adjustable parameters (note that each gas is fully characterized by its frequency-dependent susceptibility plus a single-active-electron potential) underlines the universal nature of the SC enhancement effect across the noble gases. The success of the model in explaining the most important qualitative features also indicates that the physics included in the model is indeed sufficient. We therefore conclude that the supercontinuum generation increase can be interpreted in terms of the local electric-field enhancement mediated by the seed, combined with the off-axis FWM phase-matching picture.

6. Summary and conclusions

In conclusion, using numerical simulations based on the metastable electronic state approach we have revealed the physics underlying the enhanced SC generation previously observed for optical filament propagation in noble gases in the presence of a weak seed. The simulations were shown to be in good qualitative agreement with the experiments, and examination of the angularly resolved spectrum clarified the role played by four-wave mixing in selecting an effective seed wavelength to produce enhancement. We also found that the SC spectrum was sensitive to the relative phase between the pump and seed carrier waves: This observation is a key finding of this paper and establishes the relation between the physics underlying the SC enhancement observed in Ref. [11] to recent developments in sub-cycle engineering of optical filaments. In finishing we mention that if this relative phase can be controlled this may provide a means to further improve the capability of this system as an alternative to conventional tunable sources for nonlinear spectroscopy.

Acknowledgments

This work was supported by the Air Force Office for Scientific Research under grant # FA9550-13-1-0228. EVS, DH and TE thank the National Science Foundation for support on grants ECCS-1202471 and ECCS- 1229563.

#264346 Received 29 Apr 2016; revised 16 Jun 2016; accepted 17 Jun 2016; published 24 Jun 2016